Scanning Microscopy

Volume 1994
Number 8 *The Science of Biological Microanalysis*

Article 30

5-23-1994

Confocal Fluorescence Ratio Imaging of Ion Activities in Plant Cells

M. D. Fricker
University of Oxford, fricker@vax.ox.ac.uk

M. Tlalka
University of Oxford

J. Ermantraut
University of Oxford

G. Obermeyer
Universität Salzburg, Austria

M. Dewey
University of Oxford

See next page for additional authors

Confocal Fluorescence Ratio Imaging of Ion Activities in Plant Cells

Authors

M. D. Fricker, M. Tlalka, J. Ermantraut, G. Obermeyer, M. Dewey, S. Gurr, J. Patrick, and N. S. White

Scanning Microscopy Supplement 8, 1994 (pages 391-405) 0892-953X/94$5.00+.25
Scanning Microscopy International, Chicago (AMF O'Hare), IL 60666 USA

CONFOCAL FLUORESCENCE RATIO IMAGING OF ION ACTIVITIES IN PLANT CELLS

M.D. Fricker[1*], M. Tlalka[1,2], J. Ermantraut[1,3], G. Obermeyer[4], M. Dewey[1], S. Gurr[1], J. Patrick[1], N.S. White[1]

[1]Department of Plant Sciences, University of Oxford, South Parks Road, Oxford, OX1 3RB, UK
[2]Dept. of Chemistry and Physics, Academy of Agriculture, Al. Mickiewicza 24/28, PL-30-059 Krakow, Poland
[3]Lehrstuhl für Biophysik, Institut für Biochemie und Biophysik, Biologische Fakultet, Friedrich-Schiller-Universität Jena, Philosophenweg 12, D-07443 Jena, Germany
[4]Institut für Pflanzenphysiologie, Universität Salzburg, Hellbrunner Strasse 34, A-5020 Salzburg, Austria

(Received for publication November 19, 1993, and in revised form May 23, 1994)

Abstract

Fluorescent probes allow measurement of dynamic changes of calcium and pH in living cells. Imaging using confocal scanning laser microscopy provides a route to spatially map these dynamics over time in single optical sections or in 3-D images. We have developed a dual--excitation confocal system to allow ratio measurements of pH and calcium, that compensate for changes in dye distribution, leakage and photobleaching. Application of these techniques to plant tissues is complicated by the difficulty in loading the tissues with dye. We describe a new technique to assist dye loading in intact leaves of *Lemna* using a pre-treatment with cutinase. Once within plant tissues, many dyes compartmentalise into the vacuole. We report the use of chloromethylfluorescein diacetate as an alternative to BCECF [2',7'-bis-(2-carboxyethyl)-5-(and 6)carboxyfluorescein] as a pH probe with greater cytoplasmic retention times. In addition, the confocal system allowed discrimination of signals from different compartments and permitted simultaneous measurement of vacuolar and cytoplasmic pH ratios in epidermal strips from *Hordeum*. We have developed a series of software tools to extract quantitative data from multi-dimensional images and illustrate these approaches with reference to pollen tube growth in *Lilium* and peptide-evoked changes in pH and calcium in stomatal guard cells from *Commelina* and *Vicia*.

Key Words: Calcium, confocal microscopy, cutinase, pollen tubes, pH, ratio imaging, stomatal guard cells.

* Address for correspondence:
M.D. Fricker, Dept. of Plant Sciences, University of Oxford, South Parks Road, Oxford, OX1 3RB, UK.
Phone Number: 44 865 275015
Fax Number: 44 865 275074
E-mail: FRICKER@VAX.OX.AC.UK.

Introduction

Fluorescent probes and quantitative imaging techniques provide powerful tools to map spatial heterogenity, ephemeral gradients, transients and oscillations of ion activities in living cells (For reviews see Wang and Taylor, 1989; Taylor and Wang, 1989; Mason, 1993; Farkas *et al.*, 1993). Measurements of dynamics in cytosolic calcium and, to a lesser extent, pH, have dominated the research effort in plants, in view of their fundamental role in signal transduction and ion homeostasis (Bush and Jones, 1990; Callaham and Hepler, 1991; Read *et al.*, 1992; Fricker *et al.*, 1993b; Gilroy *et al.*, 1993; Read *et al.*, 1993), though probes for other ions such as K^+, Na^+, Cl^-, Mg^{2+}, Zn^{2+} are available (Haugland, 1992). Intracellular ion measurement involves introduction of a chelating agent whose fluorescent properties alter with the ion activity. This may be a quantitative change in intensity (single wavelength dyes) or a shift in either the excitation or emission spectrum (ratio dyes) on binding to the ion of interest. The ratio of intensities, typically at wavelengths corresponding to the peak for the free and bound forms, automatically accounts for local variations in dye concentration, cell thickness, dye bleaching or leakage and is the method of choice for quantitative measurements (Bright *et al.*, 1989). Observation of tissues with resolution at the cell and sub-cellular level typically involves magnification 100-600 fold using high numerical aperture objectives. Fluorescent images are usually acquired using cameras with intensified and/or cooled detectors with a range of microscope control devices to provide rapid wavelength selection (Mason *et al.*, 1993; Bolsover *et al.*, 1993). Confocal laser scanning microscope (CLSM: Wilson, 1990; Pawley, 1995) is an alternative well established instrument that permits non-invasive blur-free optical sectioning from living tissues (White *et al.*, 1987; Shotton, 1989; Shotton and

White, 1989) with several advantages over conventional wide-field fluorescence microscopy for quantitative measurements (Williams, 1990). Removal of the out-of-focus information improves the localisation of quantitative measurements by defining a sampling volume (voxel) in the specimen and also allows sampling deep within intact tissues with a significant reduction in the contribution of autofluorescence from structures lying outside the focal plane, such as cell walls (Williams *et al.*, 1990). However, implementation of ratio measurements on CLSM instruments requires lasers with appropriate excitation wavelengths for the fluorescent probes and rigorous attention to chromatic problems to ensure correct registration of images in X,Y and Z (Fricker and White, 1992). A range of dyes are now available for key ions such as Ca^{2+} and H^+ with excitation wavelengths that coincide with readily available low-cost visible lasers. We have developed a multiple-wavelength CLSM with co-aligned excitation at 442 nm and 488 nm for (i) ratio measurements of pH using BCECF (Fricker and White, 1992; Fricker *et al.*, 1993a,b; Thiel *et al.*, 1993), (ii) single wavelength measurements of calcium using Fluo-3 (Fricker *et al.*, 1994) or (iii) ratio imaging of calcium using Fura-Red.

Measurements of pH and Ca^{2+} in plants are not straightforward, however. Dyes are exceptionally difficult to load into intact tissues by non-invasive means and once within the cell, tend to compartmentalise rapidly (Read *et al.*, 1992; Fricker *et al.*, 1993b). In a mature plant cell, the cytoplasm is a thin layer, usually less than one μm thick, sandwiched between the vacuole and the cell wall, with larger accumulations around the nucleus and chloroplasts. This geometry and the difficulty in gaining access to the tissues complicates the quantitation of weak fluorescence signals in vivo. In this paper we concentrate on the benefits and limitations of confocal microscopy for ion imaging, using examples from stomatal responses in *Commelina communis* and *Vicia faba*, pollen tube growth in *Lilium longiflorum*, infection of *Hordeum vulgare* by *Erisiphe graminis* and blue-light responses in *Lemna* and *Arabidopsis*.

Materials and Methods

Plant material, tissue preparation, dye loading and perfusion conditions.

Epidermal strips from *Commelina communis* were prepared according to Weyers and Meidner (1990) and securely fixed down with silicone grease in an open perfusion system to prevent movement during microinjection and observation (Gilroy *et al.*, 1991). The perfusion medium comprised 50 mM KCl, 1 mM MES (2-[N-Morpholino]ethanesulphonic acid) adjusted to pH 6.1 with KOH. Epidermal strips from *Vicia faba* were mounted using silicone adhesive (e.g., Corning 355--Blatt, 1991) in a similar perfusion system, leaving an optically clear window for the microscope objective and condenser. Cells were perfused with medium containing 5 mM Ca^{2+}-MES, pH 6.1 ($[Ca^{2+}]$ about 1.2 mM), 10 mM KCl. Guard cells were impaled with a fine micropipette (tip about 0.1-0.3 μm) containing 0.1-1 mM dye and loaded by iontophoresis with a continuous current of 0.1-0.5 nA for 0.5-10 min (Gilroy *et al.*, 1991) to an estimated cytoplasmic concentration of 10-80 μM. Between 60-80 % of injections loaded the cytoplasm rather than the vacuole and the difference in dye distribution between these two compartments was readily observed. Stomatal apertures ranged from 6-12 μm at the start of each experiment.

Lemna trisulca L. was obtained from the Jagiellonian University collection (Krakow, Poland) and grown according to Tlalka and Gabryš (1993). Leaves were mounted using silicone adhesive or silicone grease in similar incubation chambers to those used for the epidermal strips. Leaves were perfused with medium containing 60 mM KCl, 10 mM glutaric acid, pH 4.5. BCECF (free acid) and Fluo-3 (penta-ammonium salt) were dissolved in distilled, de-ionised water to a concentration of 1 mg ml^{-1}, adjusted to about pH 7, and stored as aliquots at -20°C. For low pH loading, dyes were diluted immediately prior to use in perfusion medium to a final concentration of 12 μM (Fluo-3) or 19 μM (BCECF). At this pH the net charge on the dyes is masked rendering them membrane permeant (Bush and Jones, 1987). BCECF-AM (acetoxylmethyl ester of BCECF) and Fluo-3-AM (1 mg ml^{-1} in DMSO (Dimethylsulphoxide)) were stored under identical conditions and diluted immediately prior to use with loading buffer (60 mM KCl, 10 mM Tris-HCl, pH 7.6) to a final concentration of 8 μM (Fluo-3-AM) or 12 μM (BCECF-AM). Tissues were incubated for varying times between 0.1-24 h. Some tissues were pre-treated with purified cutinase activities ranging from 0.1 - 10 μmol min^{-1} mg^{-1} protein for 5-30 min at pH 7.6 in Tris-buffer, and then washed in incubation buffer (Tlalka, Fricker and Dewey, unpublished). Cutinase was purified using QAE-Sephadex A-25 column chromatography from culture filtrates of *Fusarium solani f.sp.pisi* after ten days growth on cutin as the only carbon source according to Coleman *et al.* (1994). Cutinase activity was assayed using p-nitrophenylbutyrate and p-nitrophenyl palmitate as substrates (Purdy and Kolattukudy, 1975). Stock cutinase was dissolved in 50 mM sodium phosphate buffer, pH 7.6 and stored at 4°C at 1 mg ml^{-1}, equivalent to an initial activity of 100-300 μmol min^{-1} mg^{-1} protein, depending on batch. Activity declined

during storage and with increasing dilution. In some experiments probenecid (1 mM in 60 mM KCl, 10 mM PIPES (Piperazine-N,N'-bis[2-ethanesulphonic acid]), pH 6.5 with KOH) was applied for 1 h before and during dye exposure (Cole *et al.*, 1991).

Mesophyll cell protoplasts of *Arabidopsis thaliana* were prepared by enzymatic digestion of 2-6 week old leaves according to Somerville *et al.* (1981) and washed in 500 mM sorbitol, 1 mM $CaCl_2$, 10 mM MES, pH 6.0 with KOH. BCECF was loaded as the AM-ester for 2 h on ice at a concentration of 12 μM. Protoplasts were mounted in 0.8% by weight low temperature agarose.

Pollen grains from *Lilium longiflorum* were collected 2 days after flower dehiscence, and washed briefly in 5% ethanol to remove most of the pollenkitt. After concentration by centrifugation (1,000 g, 1 min), pollen grains were resuspended in culture medium (10% by weight sucrose, 1.6 mM H_3BO_3, 1 mM KCl, 0.1 mM $CaCl_2$, pH 5.6) to a final density of approximately 3000 grains ml^{-1} (Obermeyer *et al.*, 1992). Germinating grains were incubated in 1-5 μM BCECF-AM for 2-3.5 h until most tubes had reached 200-400 μm in length. The DMSO had no detectable effect on pollen germination and tube growth. Aliquots of 100-300 μl were washed by gentle centrifugation to remove extracellular indicator and transferred to acid-washed cover-slips previously coated with 0.5 % by weight poly-L-lysine.

Coleoptile strips from 6-7 day old leaves from resistant and susceptible lines of *Hordeum vulgare* RISO cultivar Carlsberg II R5678 were floated on 10 mM $Ca(NO_3)_2$ and inoculated with *Erisiphe graminis f.sp. hordei* (CC1) according to Bushnell *et al.*, (1967). Peels were loaded with BCECF-AM (12 μM) for 2 h or with chloromethyl fluorescein diacetate (CMFDA) at a concentration of 21 μM for 15 min, washed and mounted, cuticle side facing the coverslip.

In vitro and *in vivo* calibrations

A series of *in vitro* calibration curves were determined using a variety of buffers designed to mimic conditions in the cytoplasm: (i) the basal medium comprised 100 mM KCl, 20 mM NaCl, 1 mM $MgSO_4$, 10 mM MES, 10 mM HEPES (N-[2-hydroxyethyl]piperazine-N'-[2-ethanesulphonic acid), 1 μM dye adjusted with KOH to the desired pH (after Bright *et al.*, 1989), (ii) viscosity was increased by the addition of 60% sucrose (Poenie, 1990; Zhang *et al.*, 1990), (iii) hydrophobicity was altered by inclusion of 25% ethanol (Russ *et al.*, 1991), and (iv) ionic strength was altered with increasing concentrations of NaCl. Fluorescence spectra were recorded using a Perkin-Elmer LS50B fluorimeter equipped with a microtitre plate reader. *In vitro* measurements were also made using the CLSM in the same chamber as the imaging experiments using the same optics. The response of BCECF was measured between pH 6.0 and pH 8.0. The response of Fluo-3 and Fura-Red was measured in the basal media at pH 7.2 supplemented with 10 mM EGTA plus appropriate amounts of $CaCl_2$ to give the required free [Ca^{2+}] (Poenie 1990). *In vivo* calibration of BCECF was attempted using gramicidin (10 $\mu g\ ml^{-1}$ final concentration from a 10 mg ml^{-1} stock in ethanol) or nigericin (10 $\mu g\ ml^{-1}$ final concentration from a 10 mg ml^{-1} stock in ethanol) in the presence of high KCl (100 mM). For calibration of the calcium dyes in vivo, cells were permeabilized with 10 μM Ca^{2+}-ionophore, A-23187 in the presence of Ca^{2+} (1 mM). For Fluo-3 this was followed by Mn^{2+} (1 mM) to quench the fluorescence from the dye to about 8x F_{min} (Kao *et al.*, 1989; Minta *et al.*, 1989) allowing F_{min} to be calculated accurately. For Fura-Red, R_{min} was obtained directly by using EGTA (10 mM) to chelate all the Ca^{2+}.

Confocal fluorescence ratio imaging

Cells were imaged using a modified BioRad MRC-600 CLSM attached to an inverted Diaphot TMD (Nikon) microscope (Fricker and White, 1992). The excitation path has been improved to deliver co-aligned beams from five separate lasers at 633 nm laser (3.5 mW, HeNe, Spektra Physics), 543 nm (1.3 mW GreNe, Melles Griot), 514/488 nm (25 mW, argon-ion, ILT Ltd), 442 nm (11 mW, He-Cd, Omnichrome) and 325 nm (30 mW UV-HeCd, Omnichrome).

Single-mode fibre-optic coupling was used to minimise transmission of vibrations from the laser cooling fans and beam shutters to the scanning system. Collimator exit lenses provided a consistent exit beam diameter of 1.4 mm with a divergence around 0.6 mrad for all visible lines. Individual wavelengths were separately aligned via precision XY adjusters and two beam-steering mirrors. This combination of alignment optics ensured that the virtual source (fibre-output beam waist) was at an equivalent axial position for each line. Beams were combined along the same optical path via standard dichroic mirrors. The beam diameters were sufficient to fill the back aperture of the x40 and x60 objectives after expansion by the 8x eyepiece of the MRC600 CLSM. Computer controlled electronic shutters ('Uniblitz', Vincent Associates, New York) were installed in the 488-nm argon-ion and 442-nm HeCd beams to enable rapid switching (0.1s) between excitation wavelengths during ratio measurements. Neutral density filters were used to balance roughly the intensity of the two beams.

Fluo-3 was imaged using single wavelength excitation at 488 nm, BCECF and CMFDA were imaged

using sequential dual-excitation at 442 nm (the pH independent wavelength) and 488 nm (the pH dependent wavelength) with emission at >520 nm or 540±15 nm (Fricker and White, 1992; Fricker *et al.*, 1993a,b; Kurtz, 1993). Fura-Red was imaged with the same excitation for BCECF, but with emission at 635±30 nm or >600 nm. X,Y and Z alignment of images was assessed using 6 μm diameter fluorescent microspheres (Polysciences, Inc. Warrington, PA). The electronic shutters switching between the lasers were synchronised with the scanning microscope by the MPL™ instrument control program or the rationing Time-Course Software (TCSM™, BioRad Microsciences Ltd). In some experiments, non-confocal bright field images were collected simultaneously using the standard transmission detector and light-guide coupled into the second MRC600 detector channel.

Image acquisition, processing and analysis

Images were collected over a variable rectangular area slightly larger than the object with a pixel spacing of 0.24 μm (Zeiss Plan-Neofluor x25 0.8 N.A. multi-immersion lens, MRC600 zoom 3) or 0.29μm (Nikon Plan-Apo x60 1.4 N.A. oil-immersion lens, MRC600 zoom 1.5). This minimised the time taken to collect images when following changes in Ca^{2+} or pH over time. Alternatively, three-dimensional images were collected by automatically stepping the microscope focus at 1 μm intervals between each section. The sampling rates depended on the number of image lines collected and the number of frames integrated (typically four per wavelength). Acquisition of each wavelength pair took 2-5 s and sampling was repeated at 5-20 s intervals. Serial image sequences were stored initially on a RAM disc to minimise disc writing times between image acquisition at each wavelength. Images of the interaction between *Erisiphe* and *Hordeum* were collected sequentially with excitation at 442 nm and 488 nm, with simultaneous non-confocal bright field images, at 2 μm steps through the fungus and epidermal layer (typically 20-30 sections). Collection was repeated at 10 min intervals during development of the appressorial germ tube for both resistant and susceptible pathotypes, generating 4-D images.

The TCSM software allowed background subtraction and calculation of the average ratio from a number of user-defined regions during each frame scanned. Graphical presentation of the ratios from these regions allowed dynamic changes to be followed during the experiment and synchronised with treatments *via* on-screen annotation of the traces. Post-processing and calculation of ratio images was performed using the MPL™ and COMOS™ 6.03 programs (Bio-Rad Microsciences Ltd). After subtraction of the background in each wavelength image, the ratio image was calculated pixel by pixel for the 488 nm image divided by the 442 nm image. Regions below an intensity of 8-16 (0-255 scale) in the 442 nm image intensity were used to construct a mask that excluded the corresponding unreliable regions of high variance from each ratio image. Additional masking was used to exclude regions where the signal in either channel was approaching saturation (intensity greater than 240) and would thus yield distorted ratio values.

A protocol was developed to extract data from regions, such as the tip of the pollen tube, which move during the course of the experiment. A cursor was used to draw a transect along the path of the object. The intensities along the line were spatially averaged over a number of pixels normal to the track (typically 8-32) for both wavelength images. Sampling was repeated for each XY image in the time course and data from each averaged transect written into successive lines of an XTime image using MPL commands and a DOS program written by NSW. XT ratio images with threshold masking were obtained as described for the XY images. In addition, the masked ratio image was used to align the XT images: Each line of the XT image was right- or left-justified, to align a reference structure in each time point, such as the growing pollen tube tip. A vertical time-transect across this normalised XT image provided direct access to the change in ratio for any given position along the tube.

Final ratio images were pseudocolour coded using look-up tables where the ratio was represented by 254 different colours ranging from blue through green to red. The 255 intensity was reserved for unreliable regions of saturated fluorescence and coded purple to avoid ambiguity. Images in this paper are reproduced in monochrome, where white represents high $[Ca^{2+}]i$ or high pH. Images were recorded using a thermal transfer printer (CK100, colour or P78B, monochrome, Mitsubishi, Japan), photographed directly from the video monitor screen using Fuji 100 ASA daylight colour slide film, or transferred as a sequence of video animation onto an S-VHS VCR.

Chemicals

All dyes were obtained from Molecular Probes (Eugene, Oregon). Other chemicals were from Sigma (Poole, Dorset). The cutin was a generous gift of Dr JOD Coleman. Highly purified cutinase from expression of the recombinant protein in *E. coli* was a gift of Dr. PE Kolattukudy (Ohio State University Biotechnology Center, Columbus, Ohio).

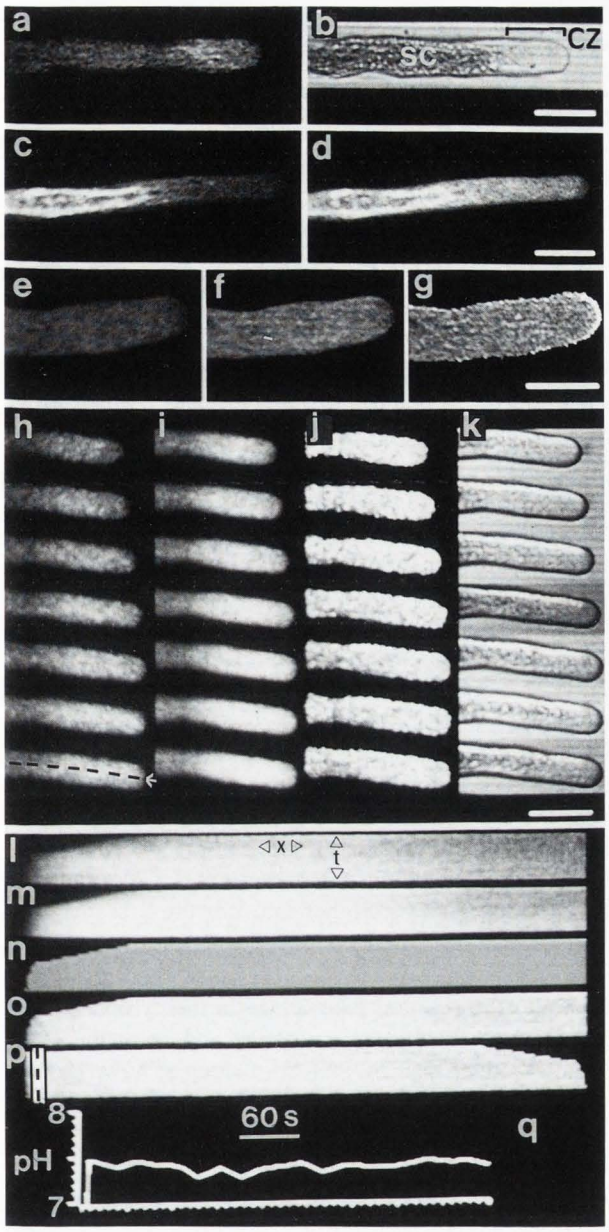

Figure 1: Confocal imaging of pH and Ca^{2+} in growing pollen tubes of *Lilium longiflorum*.

Germinating pollen tubes were loaded with dyes as the AM-ester. (*a*) single optical section of a Fluo-3 loaded tube and the corresponding bright-field image (*b*). BCECF loaded tube imaged at 442 nm (*c*) and 488 nm (*d*). Loading was allowed to continue for 3 h. A homogeneous distribution of dye is visible in the clear zone (CZ) at the tip, but, dye is visible in punctate and filamentous structures in the more basal streaming cytoplasm (SC). Rapid tube growth can cause a mismatch in the 442 nm (*e*) and 488 nm (*f*) images that gives an artifactual crescent of high pH at the tip (*g*). Reducing the interval between image collection at each wavelength alleviates this problem and pH can be followed over time: (*h*) 442 nm XY image collected at 10 s intervals (first 7 time points out of a series lasting 5 min); (*i*) corresponding 488 nm XY images; (*j*) XY ratio 488/442 images, with masking of values less than 16, white corresponds to high pH; (*k*) corresponding bright-field images. Images are averages of 4 frames collected with a 60x 1.4 N.A. oil immersion lens at the mid plane of the tube. To extract quantitative data from such a time-series, an 8 pixel wide transect was drawn along each wavelength image from tip to base (right to left) and written into successive lines of an XT (Time) image ((*l*) 442 nm, (*m*) 488 nm). The mask image of values greater than 16 is shown in (*n*) and the masked XT 488/442 ratio image in (*o*). Left justification of the masked ratio image aligns the ratio XT image to the tube tip (*p*). An 8-pixel wide transect through this image extracts the ratio value for the tip region over time (*q*), which was related to pH after calibration at the end of the experiment.

All scale bars=25 μm.

Results and Discussion

Dye loading protocols

Plant cells have proved recalcitrant to loading with fluorescent ion indicators (Read *et al.*, 1992; Callaham and Hepler, 1991; Fricker *et al.*, 1993b). We have examined a variety of approaches with varying success in different tissues. Fluo-3 and BCECF were loaded as AM-esters in pollen tubes of *Lilium longiflorum*, and hydrolysed to release active indicator in the cytoplasm (Figure 1*a,c*). However, little signal was obtained from Fura-Red-AM under identical conditions (data not shown). All three dyes were loaded into the cytoplasm of protoplasts from *Arabidopsis thaliania* subsequently immobilised in agarose, though the signal from Fura--Red was again weak (data not shown). BCECF and Fluo-3 did not enter cells in intact leaves of *Lemna trisulca* even after incubation for 30 h at external pH values between 4.5-8.0 with the dye present as free-acid or AM-ester and at concentrations from 1-10 μM (data not shown). In contrast, intracellular fluorescence was visible in a population of cells after pre-treatment of the leaf with cutinase prior to low-pH loading (pH 4.5) of the free-acid form of Fluo-3 (Figure 2*a*) or BCECF (data not shown). The number of cells loaded and the rate of loading increased directly with cutinase concentration and length of cutinase exposure. Low-pH loading was used in preference to AM-ester loading, as the residual cutinase remaining externally after the wash stages was still sufficient to partially hydrolyse the

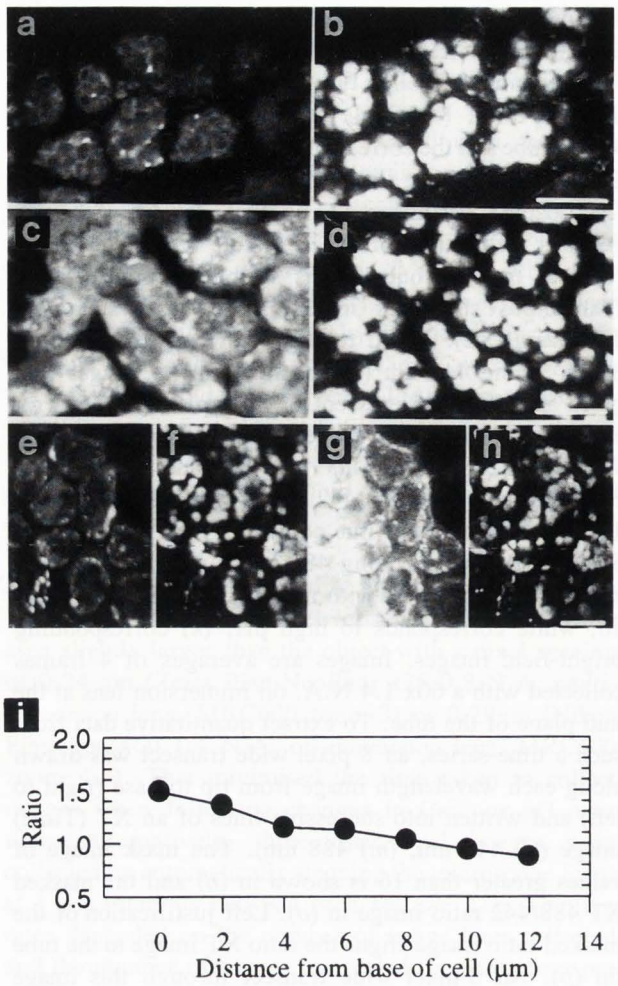

Figure 2: Cutinase pre-treatment allows loading of Fluo-3 in *Lemna*.

Leaves of untreated *Lemna* did not take up Fluo-3 by any loading technique tested and only exhibited chloroplast autofluorescence with excitation at 488 nm. However, after 10 min cutinase treatment, Fluo-3 could be loaded at pH 4.5 and accumulated in the cytoplasm of a number of cells and was imaged at 540±30 nm (*a*). The distribution of chloroplasts was monitored simultaneously with emission at 635±30 (*b*). After prolonged incubation (2 h), dye accumulated in the vacuoles (*c*). Fluo-3 retained in the cytoplasm remained sensitive to calcium, and responded to A-23187 and high external calcium levels with a dramatic increase in fluorescence after 3 min (compare *e* and *g*). The corresponding chloroplast autofluorescence images are shown in *f* and *h*. Single optical sections averaged over 4 frames collected with a x25 0.8 N.A. oil immersion lens at an approximate depth of 15-25 μm into the tissue. Scale bars = 25 μm. The change in ratio due to selective chlorophyll absorption for the pH dye, BCECF, is shown as a graph of the ratio (488/442) averaged for the cytoplasm of a single mesophyll cell in 7 successive optical sections taken at 2 μm intervals from the base of the cell. There was a progressive shift to lower values from the base to the mid region of the cell. We think this reflects differential absorption of the 442 nm versus the 488 nm excitation beam as it passes through the chloroplasts, giving a higher ratio for the first image in the sequence near the base of the cell.

AM-esters. Cutinase treatment did not alter the rate of chloroplast re-orientation in *Lemna* (data not shown).

Many other intact tissues, including roots, intact leaves, epidermis, petals and anthers from a range of species, could not be loaded by non-invasive techniques, or rapidly compartmentalised dyes into vacuoles. We have investigated an alternative technique to measure pH using the dye CMFDA. By analogy with parent fluorochrome, fluorescein diacetate (FDA), this is readily membrane permeant and the acetate groups cleaved to release free dye in the cytoplasm of plant cells. The chloromethyl group renders the dye non-fluorescent until catalytically conjugated to glutathione (GSH) by glutathione transferase (GST). CMFDA thus provides an indication of the level of GSH and the activity of GST in live cells, as well as providing a ratioable pH-sensitive indicator, due to the fluorescein group (Figure 3). We are currently assessing the specificity of this reaction for GSH in plant cells by comparison with the more commonly used dye, mono-chlorobimane (Fricker and May, unpublished). In addition, we are calibrating the pH response of the fluorescein-glutathione adduct. In principle, the reaction takes place in the cytoplasm and the observed retention time of the adduct in the cytoplasm is longer than BCECF for example, however, we have also observed accumulation of the adduct in the vacuole (Figure 3), in a cell- and tissue-specific manner (Fricker and May, unpublished). This may reflect operation of a GSH-based de-toxification pathway via a specific tonoplast transporter.

In guard cells of *Commelina communis* or *Vicia faba*, microinjection provided direct access to the cytoplasm and allowed introduction of Fluo-3, Indo-1, BCECF or Fura-Red (Figure 4 *a,b,c,f* respectively). Microinjection was very time consuming, however, and stringent controls were required to ensure that the guard cells were not disrupted by this invasive loading technique. One advantage of the confocal imaging system is that the loading electrode can remain in place during the experiment (Figure 4*a*) as the massive out-of-focus signal from dye in the pipette is excluded by the confocal optics. This also opens the possibility of simultaneous electrophysiological measurements.

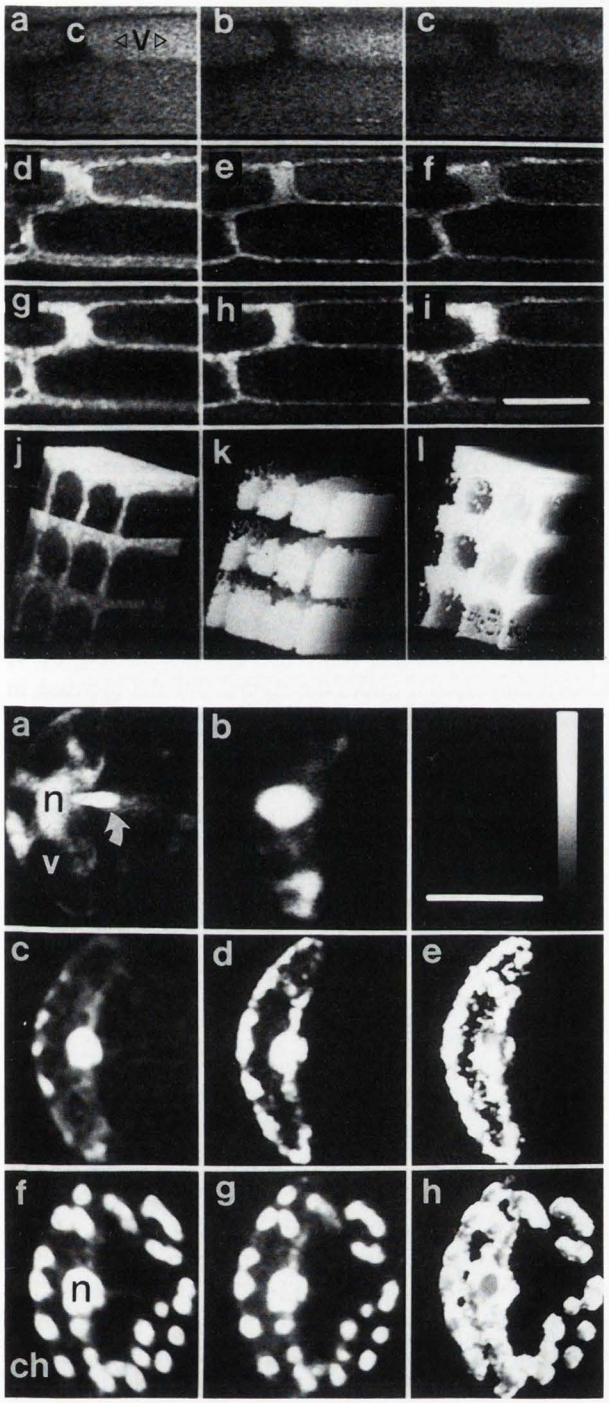

Figure 3: 4-D pH ratio images using CMFDA of epidermal cells from *Hordeum vulgare* infected by *Erisiphe graminis f.sp. pisi* during development of the appresorial germ tube.

Epidermis was loaded with CMFDA and XYZ images collected at 2 μm intervals through the fungus and the epidermal cell layer, with repeated sampling at 10 min intervals. A single optical section near the mid-plane of the epidermal cell layer is shown for the first three time points with excitation at 442 nm (*a-c*) and 488 nm (*d-f*). The corresponding ratio images for 488 nm/442 nm are shown in (*g-i*). After this long loading time, the fluorescent glutathione adduct has compartmentalised into the vacuole, though some signal remains in the cytoplasm. The ratio images clearly indicate a difference in ratio between these two compartments. A representation of the complete 4-D image is shown in (*j*). Serial optical sections for each time-point are laid horizontally, viewed from the bottom left corner, and stacked to form a 3-D model. The three models in turn are stacked in order, with the first time-point at the top, and are viewed as a tilted block. The strong signal from the top surface is probably due to extracellular dye binding to the cuticle, which unfortunately obscures the fungal spore and appressorial germ tube lying on the surface. The 4-D ratio image can be segmented using a simple threshold to visualise regions of low ratio and presumed low pH (*k*) or high ratio and presumed high pH (*l*). These images are height-coded where white represents an occurrence of the threshold near the viewer and black, further away. The segmented regions in k and l correspond to the morphology expected of the vacuoles and the cytoplasm, respectively. Images were collected with a x60 1.4 N.A. oil immersion lens. Scale bar=25 μm.

Figure 4: Imaging of calcium and pH in stomatal guard cells of *Commelina communis* and *Vicia faba*.

Single guard cells in the stomatal complex were iontophoretically microinjected with the free-acid form of each dye. (*a*) Single optical section averaged over 4 frames of Fluo-3 loaded guard cell from *Vicia faba* with the injection micro-electrode still in place (arrow). (*b*) Single optical section near the base of a guard cell from *Commelina communis* loaded with Indo-1 with excitation at 325 nm and emission at > 400 nm. (*c-h*) Simultaneous dual-excitation, dual-emission imaging of pH and calcium using BCECF and Fura-Red, respectively. Single optical sections averaged over 8 frames near the mid-plane of a single guard cell from *C. communis* with excitation at 442 nm (*c&f*) or 488 nm (*d&g*) and emission to 540$\pm$30 nm (*c&d*) or >600 nm (*f&g*). The ratio images were calculated as 488/442 for BCECF where white equates to higher pH (*e*) and 488/442 for Fura--Red, where white equates to low calcium (*h*). The chloroplasts are visible by autofluorescence in the red emission channel but can be distinguished easily from dye signal as the ratio does not alter during calibration. Scale bar=25 μm. The intensity wedge is not calibrated in these images.

Dye distribution and compartmentalisation

Optical sectioning using CLSM showed that dye signals were not uniformly distributed in the cytoplasm for any of the tissues studied. The nucleus accumulated 6-10 fold higher concentrations of fluorochrome (e.g., Figure 4). Punctate fluorescence from dye in endoplasmic reticulum, mitochondria or other small vesicles was apparent in some tissues, such as pollen tubes (Figure 1 *c,d*), but not others, such as guard cells (Figure 4). In pollen tubes, BCECF gave a relatively homogeneous fluorescence in the clear zone (CZ) near the tip with excitation at 442 nm, equivalent to an even dye distribution in the cytoplasm. However, vesicles and strands were visible in the streaming cytoplasm (SC) basal from the tip. This signal probably arises from compartmentalisation of the free-acid form of the dye after hydrolysis as it also occurs after microinjection (Read *et al.*, 1992). The amount of punctate fluorescence was variable, but tended to increase with longer incubation in the AMester (Figure 1 *c,d*). The punctate regions had differing ratios to the clear zone, also indicative of localisation of the dye in different compartments (data not shown). Preliminary experiments on epidermis from *Hordeum* coleoptiles indicates that the ratio from the vacuolar and cytoplasmic compartments determined by optical sectioning was markedly different after sequestration has occurred (Figure 3*g-i*). We have not yet assessed how well these ratio values can be related to the difference in pH between these compartments, though the vacuolar ratio is unlikely to be very reliable since the expected pH (pH 5.0-5.5) is outside the useful range for BCECF. In *Lemna*, the anion transport inhibitor probenecid (Cole *et al.*, 1991) was partially effective in preventing vacuolar compartmentalisation, but required very high (1-2.5 mM) concentrations and had significant effects on sub-cellular morphology (Oparka *et al.*, 1991). The effectiveness of probenecid may have been reduced by the low pH required for acid loading, as the drug tends to precipitate below about pH 6.0.

Data collection: signal-to-noise, sampling speed and spatial resolution

For measurements on live cells, the concentration of fluorochrome introduced should be kept low to minimise buffering of the ion involved and any potential non-specific chemical or photo-chemical side-effects. The number of photons emitted per voxel and registered by the detection photomultiplier is often less than eight per scan and requires photon-counting for accurate quantitation. This reflects the limited number of true grey-level intensities that can be distinguished, rather than the nominal 256 separate levels resulting from digitisation of the analogue signal to 8-bits. In addition, we routinely exclude signals within about $\sqrt{255}$ of saturation (240) and mask out signals below 16 as the variance in the ratio becomes excessive, further reducing the useable dynamic range of the detector system. An increase in signal-to-noise can be achieved with temporal averaging, spatial averaging, increasing the wavelength bandwidth of the detector (which decreases the sensitivity to dye responses) or increasing the aperture of the pinhole detector on instruments where this is variable. We have found setting 5 on the BioRad MRC600 to be acceptable for ion measurements. Sheppard (1993) has reported a near linear increase in signal to 70% of the maximum, with the aperture set to the 1st minimum of the Airy disc for an on-axis confocal configuration, with only a 30-40% increase in the optical section thickness. These figures cannot be transferred directly to the BioRad system as the optical path used to achieve confocal sectioning is different. However, Lemasters *et al.*, (1993) have measured optical section thickness on the BioRad instrument and show that there is no substantial increase in resolution below an aperture setting of 4, though they do not quote the figures for the increase in signal, or signal to noise ratio, with the higher aperture settings.

The maximum sampling speed (about 2 μs voxel^{-1}) is dependent on the scanning hardware and photomultiplier integration circuitry and this determines the most rapid transients that can be reliably measured, i.e., at a sampling rate at least twice the maximum transient frequency. In experiments where temporal resolution is critical, the area scanned can be reduced to a single line (about 2 ms) or even a single point (about 2 μs), though 16-64 scans are usually averaged to increase the signal to noise. In excitation ratio experiments there is a finite interval between collection of each wavelength image, during which time there must be minimal change in the sample for reliable rationing. Artifacts from organelle or specimen movement are particularly pronounced with confocal systems because of the reduced depth of field.

The growing pollen tube tip advanced at up to 0.2 μm s^{-1} at room temperature (18-22°C). Slow sampling and the delay between each wavelength during disc writing up to about 5 s was sufficient to give mis-regist- ratio between the two wavelength images and initially resulted in a crescent of dramatically different ratio at the tube tip (Figure 1*e-g*). Sampling intervals between each wavelength were reduced to sub-second levels with fewer frames averaged and the use of a RAM disc for rapid image storage to minimise the temporal sampling artifact (Figure 1*h-k*). Signal to noise was then increased by averaging a thick (8-32 pixel) curve transect along the centre of the tube for each time point to construct a single XT (X vs Time) image for each wavelength

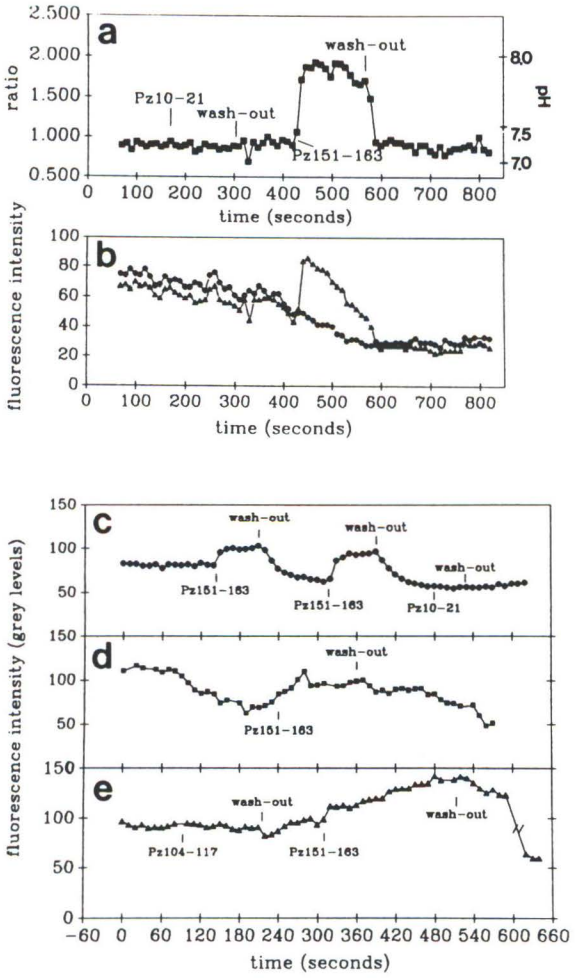

Figure 5: Changes in pH and calcium in stomatal guard cells in response to peptides derived from the auxin binding protein

Guard cells from *vicia faba* were loaded with BCECF (*a,b*) or Fluo-3 (*c-e*) by iontophoretic microinjection and imaged at >520 nm with sequential excitation at 442 nm and 488 nm at a focus plane at the mid plane of the cell, using a Nikon Fluor 40x 0.85 N.A. lens. Cells were exposed to peptides derived from near the N-terminus (Pz10-21) or the C-terminus (Pz151-163) of the auxin binding protein from *Zea mays* at the points indicated. (*a*) Time course of changes in ratio derived from the averaged area of cytoplasm near the nucleus, with a pH scale based on *in vivo* calibration with nigericin and high K^+ at the end of the experiment. (*b*) Time course of changes in fluorescence with excitation at 442 nm (●) and 488 nm (■). The 442 nm signal represents dye concentration and illustrates the decline in dye from leakage and photobleaching during the experiment. (*c-e*) Three replicate experiments showing the change in fluorescence of Fluo-3 with time for a region near the nucleus extracted using the transect analysis (see text for details) during exposure to the C-terminal peptide, Pz151-163, at the points indicated.

(Figure 1*l,m*). An XT ratio image was calculated as the 488 nm-XT/442 nm-XT image (Figure 1*o*) and masked at values less than 16 in the 442 nm-XT image (Figure 1*n*). Values for changes in pH at the tube tip were extracted with a second thick transect through the XT-ratio image after re-aligning to the pollen tube tip for each time point (Figure 1*p*), and displayed graphically (Figure 1*q*). This alignment was necessary so that the averaging normal to the transect only occurred in the spatial (X) dimension.

In guard cells, the sampling frequency was fairly low (0.1 Hz), as no rapid transients have been reported for this tissue to date using sampling rates of up to 1 Hz (e.g., Gilroy *et al.*, 1991). The high spatial resolution of the confocal microscope, however, was used to allow unambiguous discrimination of cytoplasmic signals even in the presence of much higher signals from the nucleus and auto-fluorescence from the chloroplasts (Figure 4*h*). Using software tools to extract quantitative data from such images, an original 3-D XYT image file was typically reduced from several Mbyte, to a set of numerical values that were displayed graphically or output for statistical comparison with other treatments (Figure 5).

Calibration

Most in vivo calibrations involve selective permeabilisation of the plasma membrane with an ionophore to allow equilibration of internal ion activities with defined external levels. We have encountered three major difficulties with this approach. Firstly, dye often leaks rapidly out of ionophore clamped cells or is compartmentalised into the vacuole, where the prevailing pH, viscosity and ionic conditions in the vacuole are markedly different from the cytoplasm and affect the K_d of the dye, which is used to calculate free ion concentration from the following equations.

for a single wavelength dye:

$$[\text{ion}] = K_d(F-F_{min})/F_{max}-F) \qquad (1)$$

F= intensity of fluorescence measured, F_{min}= fluorescence of free dye, F_{max}= fluorescence of saturated dye.

for a ratio dye:

$$[\text{ion}] = K_d\,[S_f(R-R_{min})]/[S_b(R_{max}-R)] \qquad (2)$$

$R = F_{\lambda 1}/F_{\lambda 2}$ where λ is the excitation wavelength
R_{min}= fluorescence ratio of free dye

R_{max} = fluorescence ratio of saturated dye
S_f = fluorescence of free dye at λ_2
S_b = fluorescence of bound dye at λ_2

It is not clear how calibrations under these conditions relate to cytoplasmic activities. In addition, dilution into the large volume of the vacuole caused a decrease in the signal intensity by an unknown factor, which can only be corrected for ratio dyes. Thirdly, the ionophore/ion clamping protocol has a dramatic effect on the subcellular morphology (and presumably physiology) in some cell types. In pollen tubes, addition of nigericin causes abrupt cessation of growth and a surge of vesicles towards the tip. Further increasing the external pH to 8.0 often caused the tube to burst. Thus, precise or accurate quantitation using a single wavelength is difficult, though it is appropriate to determine the direction and relative magnitude of changes. Calibration of ratio dyes appears to be consistently more reproducible. Thus, a calibration scale derived from in vivo measurements is provided for pH measurements for experiments on pollen tubes (Figure 1) and stomatal guard cells (Figure 5). The Ca^{2+} changes shown in Figure 5 for the single wavelength dye Fluo-3 can be estimated as an increase of 400-800 nM above resting (about 230 nM) based on (i) *in vivo* calibration at the end of the experiment and (ii) a single exponential fit to the resting level signal before stimulation to partially correct for dye leakage and bleaching.

Artifacts

We have encountered four other potential artifacts that are particularly obvious using confocal microscopy, but may occur in conventional ratio imaging experiments and remain undetected. We have not yet rigorously characterised the errors introduced in quantitation. Fluorescence ratio techniques, by definition, involve three wavelengths which must be coincident at the sample and at the detector if the confocal geometry is to be successful. Lateral and axial chromatic aberration causes displacement of one or more wavelengths, distortion of the point spread function, loss in detection efficiency and mis-registration of images. Lateral chromatic aberration does not seem to be a major problem for small images in the center of the field of view. Axial chromatic aberration is more significant, however. Conventional Plan-Apo microscope objectives are corrected for three wavelengths, typically in the blue (e.g., hydrogen F-line at 486 nm), green/yellow (e.g., helium d-line at 587 nm) and red (e.g., hydrogen C-line at 656 nm). The relative focus shift for intermediate wavelengths depends on the design of the objective. The overall focus shift depends on the sum of all the axial chromatic aberrations in the light path. We have measured the plane response function for a number of wavelengths for our multiple laser system (325 nm, 442 nm, 488 nm, 514 nm and 633 nm) and a commercial multi-line laser system (488 nm, 567 nm and 649 nm) (Fricker and White, 1992). With a Nikon 60x 1.4 N.A Plan-Apo lens, the maximum focus shift was 0.3 μm (half the minimum section thickness with the confocal detection aperture fully closed) between the blue and red wavelengths. In practice, increasing the detection aperture diameter to increase the signal (see section iii) relaxes the depth of field and generates increased overlap between the voxels sampled at different wavelengths. In the fibre-optic coupled system described here, the virtual source of the exit beam waist can be readily adjusted to compensate for minor axial chromatic aberration and there is facility to introduce additional pre-focussing lenses to correct for longer focus shifts.

The next three problems arise from interaction of the excitation and emission wavelengths with the specimen. Light attenuation is a complex function of wavelength, local refractive index variation, absorption and scattering, and results in a wavelength- and depth-dependent loss of the excitation and emission intensities (Fricker and White, 1992). The most significant depth--dependent attenuation arises from spherical aberration due to mis-match of the refractive index between immersion fluid, sample and perfusion medium (White, Wood, Errington and Fricker, in preparation). An additional wavelength dependent component is superimposed on this net attenuation and, in preliminary studies, suggested a variation in the ratio for a constant ion activity with a shift in favour of signal from longer wavelengths (Fricker and White, 1992). The absorption problem results from the extensive array of pigments prevalent in plant cells. Chloroplasts are the most notable examples, with substantial absorption by chlorophylls of blue and red wavelengths and variable absorption of other wavelengths depending on the type and quantity of accessory pigments. Differential absorption of blue (442 nm) versus blue/green (488 nm) by chloroplasts gives an increase in the ratio for BCECF towards apparently more alkaline values (Dixon *et al.*, 1989; Fricker *et al.*, 1993a). In small cells with few chloroplasts such as guard cells, the spatial resolution of the confocal microscope can be used to discriminate areas occupied by chloroplasts relatively easily. In spherical protoplasts or leaf mesophyll, where large numbers of chloroplasts are distributed more randomly around the periphery, these effects become more pronounced (Figure 2*i*). Ratio values determined for a single plane over time still provide a reliable description of changes in pH, but the absolute value of the ratio becomes more

difficult to calibrate. The final problem relates to the physiological response that the excitation or emission wavelengths used for imaging may trigger in the specimen. For example, chloroplasts can be readily imaged with excitation at 442 nm, but this may also trigger blue-light dependent responses. Fortunately, chlorophyll also fluoresces with excitation at 633 nm or 647 nm, allowing chloroplast movements to be tracked without triggering the blue-light dependent pathway. Equally, however, these red wavelengths may stimulate phytochrome mediated responses in some tissues.

Biological applications of ion measurements: pH and Ca^{2+} in stomatal guard cells

We have used dual-excitation confocal imaging of BCECF to investigate the presence and activity of the putative plasma membrane docking protein thought to be the first link in transduction of auxin stimulus after association with the auxin binding protein (ABP). The biological activity of synthetic peptides derived from predicted hydrophilic surface regions of the ABP was screened for effects on cytosolic pH, Ca^{2+} and membrane transporters (Thiel *et al.*, 1993; Fricker *et al.*, 1994). The 12 amino-acid peptide corresponding to the C-terminal portion of the ABP from *Zea mays* (Pz151--163) caused rapid and reversible increases in cytosolic pH from resting levels (pH 7.2-7.5) up to around pH 7.8 (mean ΔpH 0.4 ± 0.1, n=6) (Figure 5*a,b*) (Thiel *et al.*, 1993). The time course was variable with the most rapid responses essentially complete within 20 s and the mean half-time of 54 ± 33 s. Cytosolic pH values stabilised at the new pH and were maintained over the longest period examined (120 s), but returned to resting pH levels upon washout of the peptide with a mean half-time of 150 ± 80 s. We have not yet examined longer term kinetics of the pH response. Five other ABP-peptides tested did not give detectable changes in pH, even in cells shown to respond to Pz151-163 (e.g., Figure 5 *a,b*). Pz151-163 also caused changes in cytosolic calcium levels of varying magnitude (Figure 5*c*) (Fricker *et al.*, 1994). Calibration of the signal was complex (see above). An estimate of the magnitude of the change in Ca^{2+} was obtained from *in vivo* calibration at the end of the experiment with A23187 followed by Mn^{2+}, using a single falling exponential fit to the resting fluorescence level before stimulation to partially compensate for the loss in signal from dye leakage or bleaching suggest rises typically of 400-800 nM above resting. The absolute figures should be treated with some caution, however. The response half-time was also variable (35 ± 19 s, n=4), as was the decay time upon washout of the peptide (90 ± 43 s, n=4). Repeated exposure of the same cell to Pz151-163 resulted in a similar pattern of response (Figure 5*c*). In trials so far of two of the other peptides, no marked changes in fluorescence were recorded, but it was difficult to discriminate small perturbations from the background decay rate using a single wavelength dye.

The excitation wavelengths used for dual-excitation ratio imaging of BCECF are also appropriate for excitation of the visible calcium ratio dye Fura-Red, whose emission maximum (630 nm) is sufficiently distinct from BCECF to allow simultaneous dual-emission detection (Figure 4*c-h*). The quantum efficiency of Fura-Red is significantly lower than the single wavelength calcium dyes and currently we have to load a higher concentration (50-100 μM) to obtain a useable signal. Fura-Red also has an additional emission peak around 540 nm with excitation at 442 nm, which is still responsive to calcium. This causes potential bleed-through from the Fura-Red channel into the BCECF channel, in addition to the expected bleed-through of the BCECF into the longer wavelength channel. In practice, these errors can be minimised by careful balancing of the laser intensities, dye concentrations and filter combinations, though it is difficult to maintain all four signals within the dynamic range of the system during the experiment and calibration procedure. Combination of pH and Ca^{2+} measurements should allow us to distinguish the order of changes in these key signal intermediates, which is vital to understand how the complete signal transduction network is co-ordinated.

Conclusions

CLSM reduces a number of problems associated with quantitative measurements of free ion concentrations using camera-based imaging or photometric measurements and also highlights several potential sources of imaging artifact that would normally be obscured by the poor spatial sampling of these techniques. Removal of out-of-focus blur by high-resolution optical sectioning makes quantitation more accurate for the defined volume sampled in the specimen, without contribution of signals from neighbouring structures (Bolsover *et al.*, 1993). In plant cells, one of the most notable benefits is the resulting low or negligible level of autofluorescence from structures such as the cell walls over-lying the cytoplasm. This is important, as correction for spatially heterogeneous autofluorescence in conventional wide-field camera images is difficult, particularly for specimens that changes shape over time, such as a pollen tube or a stomatal guard cell (Gilroy *et al.*, 1991), or where there is considerable cytoplasmic streaming and organelle movement. The relatively small and constant probe volume, in the range of 0.4

(μm)(x)0.4 (μm)(x)1.2 μm in XY and Z, also decreases the effect of gross differences in signal from variation in cell thickness, as long as the dye loaded compartment exceeds the voxel volume. This improves quantitation and calibration of single wavelength dyes. The restricted depth of field does make measurements very sensitive to signal variation due to specimen movement, however. In conventional wide-field images small displacements up to about 1 μm are disguised in the out-of-focus blur, whereas in confocal microscopy an equivalent shift would effectively sample a non-overlapping optical section.

Out-of-focus blur removal also allows deeper sampling of intact tissues such as whole leaves from *Lemna* and even interactions between two cell types in the *Hordeum* - *Erisiphe* example. The major difficulty here remains development of appropriate loading protocols to introduce the dye into the cytoplasm of a sufficient number of cells. Treatment with cutinase provided an additional tool to aid loading into some intact plant tissues without perturbating indicators of cell function, such as cytoplasmic streaming and chloroplast re-orientation. Cutin is a polyester of cross-linked C16 and C18 fatty acids and occurs embedded in a soluble mixture of waxes associated with the pectinaceous layer of the secondary plant wall (Kolattukudy, 1981). We have not determined the extent of cutinisation for *Lemna*, however, typically the upper epidermis in the *Lemnaceae* differs considerably from the lower, being more highly cutinised and un-wettable (Hillman, 1961). The concentration and exposure time to cutinase in this study would have been insufficient to hydrolyse many of the ester bonds, so we predict the increased dye uptake is through hydrophilic routes opened in the cutin layer by cleavage of a relatively small number of bonds. Cutinase may thus provide increased access to the plasma membrane and allow subsequent low-pH loading of ion indicators. This treatment proved effective in previously recalcitrant tissues and may represent an enzymatic equivalent to the harsher abrasion techniques or 'wax' removal protocols used in other tissue studies (Gehring *et al.*, 1990;a,b). As the cutinase gene has been isolated, cloned and functional cutinase expressed in *E. coli* (Abergel *et al.*, 1990), routine use of this technique is now feasible.

The problems associated with calibration of the dyes have been extensively discussed (Callaham and Hepler, 1991; Read *et al.*, 1991; Bolsover *et al.*, 1993; Fricker *et al.*, 1993b). One neglected aspect is perhaps the reason for attempting a quantitative calibration. In plant tissues we are not yet in a position to ascribe significance to most of the changes in Ca^{2+} and pH that are reported for many tissues, as the relationship between Ca^{2+} or pH change and response remains to be defined. However, the relevant biological information is not just the absolute level of Ca^{2+} or pH measured, but whether the changes reported have any physiological role. Controlled injection of ions (e.g., Zhang *et al.*, 1990) or the use of caged-compounds to artificially modulate ion levels (e.g., Adams and Tsien, 1993; Kao and Adams, 1993; Gilroy *et al.*, 1990), are needed to allow direct correlation between the fluorescence change measured and the physiological response.

The final points for consideration are the tools required to visualise and extract quantitative data from increasingly large and complex data sets. We have developed certain application specific tools to display and analyse dual-wavelength XYT images (e.g., Figs. 1 and 5). The next generation of data includes multiple-wavelength XYT images (e.g., Figure 4*c-h*) and timelapse sampling in three dimensions to generate multiplewavelength XYZT images (e.g., Figure 3). We are currently exploring a number of possibilities to visualise and extract biologically useful data from such complex images (Figure 3*j-l*).

Acknowledgements

N.S.W. thanks SERC and Dept. Plant Sciences for financial support. M.T. was in receipt of a SOROS scholarship, J.E. a scholarship from the Studienstiftung des Deutschen Volkes and G.O. a British Council travel award. This work was funded by grants from the Nuffield Foundation, Royal Society and AFRC to M.D.F.; and SERC grants to N.S.W. & M.D.F., and to D.M. Shotton, Zoology Dept. Oxford. We also thank Bio-Rad Microsciences Ltd, Spindler and Hoyer Ltd. and Lambda Photometrics for technical information and the loan of equipment.

References

Abergel C, Martinez C, Fontecilla-Camps J, Cambillau C, de Geus P, Lauwereys M (1990) Crystallization and preliminary X-ray study of a recombinant cutinase from *Fusarium solani f.sp. pisi*. J Mol Biol **215**: 215-216.

Adams SR, Tsien RY (1993) Controlling cell chemistry with caged compounds. Ann Rev Physiol **55**: 755-784.

Blatt MR (1991) Primer in plant electrophysiology. In: *Methods in Plant Biochemistry* (Hostettmann K, ed) Academic Press, New York, **6**: 281-321.

Bolsover SR, Silver RA, Whitaker M (1993) Ratio imaging measurement of intracellular calcium and pH. In: *Electronic Light Microscopy* (Shotton DM, ed) Wiley-Liss, New York, pp 181-210.

Bright GR, Fisher GW, Rogowska J, Taylor LD (1989) Fluorescence ratio imaging microscopy. Methods Cell Biol **30**: 157

Bush DS, Jones RL (1987) Measurement of cytoplasmic calcium in aleurone protoplasts using Indo-1 and Fura-2. Cell Calcium **8**: 455-472.

Bush DS, Jones RL (1990) Measuring Intracellular Ca^{2+} levels in plant cells using the fluorescent probes, Indo-1 and Fura-2. Plant Physiol **93**: 841-845.

Bushnell WR, Dueck J, Rowell JB (1967) Living haustoria and hyphae of *Erisiphe graminis f.sp. hordei* with intact and partly dissected host cells of *Hordeum vulgare*. Can J Bot **45**: 1719-1732.

Callaham DA, Hepler PK (1991) Measurement of free calcium in plant cells. In: *Cellular Calcium: A Practical Approach* (McCormack JG, Cobbold PH, eds) IRL Press, Oxford, pp 383-410.

Cole L, Coleman J, Kearns A, Morgan G, Hawes C (1991) The organic anion transport inhibitor, probenecid, inhibits the transport of Lucifer Yellow at the plasma membrane and the tonoplast in suspension-cultured plant cells. J Cell Sci **99**: 545-555.

Coleman JOD, Hiscock SJ, Dewey FM (1994) Monoclonal antibodies to purified cutinase from *Fusarium solani f.sp. pisi*. Physiological Molecular Plant Pathology **43**: 391-401.

Dixon GK, Brownlee C, Merrett MJ (1989) Measurement of internal pH in the coccolithophore *emiliania huxleyi* using2',7'-bis-(2-carboxyethyl)-5(and6)carboxyfluorescein acetoxymethylester and digital imaging microscopy. Planta **178**: 443-449.

Farkas DL, Baxter G, BeBasio RL, Gough A, Nederlof MA, Pane D, Pane J, Patek DR, Ryan KW, Taylor LD (1993) Multimode light microscopy and the dynamics of molecules, cells, and tissues. Ann Rev Physiol **55**: 785-817.

Fricker MD, Blatt MR, White NS (1993a) Confocal ratio imaging of pH in plant cells. In: *Biotechnology Applications of Microinjection, Microscopic Imaging and Fluorescence* (Bach PH, Reynolds CH, Clark JM, Poole PL, Mottley J, eds) Plenum Press. New York, pp 153-163.

Fricker MD, Tester M, Gilroy SG (1993b) Fluorescent and luminescent techniques to probe ion activities in living plant cells. In: *Fluorescent and Luminescent Probes for Biological Activity: A Practical Guide to Technology for Quantitative Real-Time Analysis* (Mason WT, ed) Academic Press, London. pp 361-378.

Fricker MD, White NS (1992) Wavelength considerations in confocal microscopy of botanical specimens. J Microscopy **166**: 29-42.

Fricker MD, White NS, Thiel G, White I, Millner P, Blatt M (1994) Peptides derived from the auxin binding protein elevate Ca^{2+} and pH in stomatal guard cells of *Vicia faba*: a confocal fluorescence ratio imaging study. In: *Membrane Transport in Plants and Fungi: Molecular Mechanisms and Control* (Blatt MR, Leigh RA, Sanders D, eds) SEB Symposium Series 48, Company of Biologists Ltd, Ca,bridge, pp 215-228.

Gehring CA, Williams DA, Cody SH, Parish RW (1990a) Phototropism and geotropism in maize coleoptiles are spatially correlated with increases in cytosolic free calcium. Nature **345**: 528-530.

Gehring CA, Irving HR, Parish RW (1990b) Effects of auxin and abscisic acid on cytosolic calcium and pH in plant cells. Proc Natl Acad Sci USA **87**: 9645-9649.

Gilroy S, Bethke PC, Jones RL (1993) Calcium homeostasis in plants. J Cell Sci **106**: 453-462.

Gilroy SG, Fricker MD, Read ND, Trewavas AJ (1991) Role of calcium in signal transduction of *Commelina* guard cells. Plant Cell **3**: 333-344.

Gilroy SG, Read ND, Trewavas AJ (1990) Elevation of cytoplasmic calcium by caged calcium or caged inositol triphosphate initiates stomatal closure. Nature **346**: 769-771.

Haugland RP (1992) *Handbook of Fluorescent Probes and Research Chemicals*. 5th Edition. Molecular Probes, Inc. Eugene, Oregon.

Hillman WS. (1961) The Lemnaceae, or duckweeds. A review of the descriptive and experimental literature. Bot Rev **27**: 221-287.

Kao JPY, Harootunian AC, Tsien RY (1989) Photochemically generated cytosolic calcium pulses and their detection by Fluo-3. J Biol Chem **264**: 8179-8184.

Kao JPY, Adams SR (1993) Photosensitive caged compounds: design, properties, and biological applications. In: *Optical Microscopy: Emerging Methods and Applications* (Herman B, Lemasters JJ, eds) Academic Press, San Diego, pp 27-86.

Kolattukudy PE (1981) Structure, biosynthesis, and degradation of cutin and suberin. Ann Rev Plant Physiol **32**: 539-567.

Kurtz I (1993) Dual-excitation confocal fluorescence microscopy. In: *Fluorescent and Luminescent Probes for Biological Activity: A Practical Guide to Technology for Quantitative Real-Time analysis* (Mason WT, ed) Academic Press, London, pp 259-263.

Lemasters JJ, Chacon E, Zahrebelski G, Reece JM, Nieminen A-L (1993) Laser scanning confocal microscopy of living cells. In: *Optical Microscopy: emerging methods and applications* (Herman B, Lemasters JJ, eds) Academic Press, San Diego, pp 339-354.

Mason WT (ed) (1993) *Fluorescent and Luminescent Probes for Biological Activity: A Practical Guide to Technology for Quantitative Real-Time Analysis.* Academic Press, London.

Mason WT, Hoyland J, Davison I, Carew M, Somasundaram B, Tregear R, Zorec R, Lledo PM, Shankar G, Horton M (1993) Quantitative real-time imaging of optical probes in living cells. In: *Fluorescent and Luminescent Probes for Biological Activity: A Practical Guide to Technology for Quantitative Real-Time analysis* (Mason WT, ed) Academic Press, London, pp 161-195.

Minta A, Kao JPY, Tsien RY (1989) Fluorescent indicators for cytosolic calcium based on rhodamine and fluorescein chromophores. J Biol Chem **264**: 8171-8178.

Obermeyer G, Lützelschwab L, Heumann H-G, Weisenseel MH (1992) Immunolocalization of H^+-ATPases in the plasma membrane of pollen grains and pollen tubes of *Lilium longiflorum*. Protoplasma **171**: 55-63.

Oparka KJ, Murant EA, Wright KM, Prior DAM (1991) The drug probenecid inhibits the vacuolar accumulation of fluorescent anions in onion epidermal cells. J Cell Sci **99**: 557-563.

Pawley JB (1995) *Handbook of Confocal Microscopy*. 2nd Edition, Plenum Press, New York. 246 p.

Poenie M (1990) Alteration of intracellular fura-2 fluorescence by viscosity: A simple correction. Cell Calcium **11**: 85-92.

Purdy RE, Kolattukudy PE (1975) Hydrolysis of plant cuticle by plant pathogens. Purification, amino acid composition and molecular weight of to isozymes of cutinase and a non-specific esterase from *Fusarium solani f.sp. pisi*. Biochemistry **14**: 2824-2832.

Read ND, Allan WTG, Knight H, Knight MR, Malho R, Russell A, Shacklock PS, Trewavas AJ (1992) Imaging and measurement of cytosolic free calcium in plant and fungal cells. J Microsc **166**: 57-86.

Read ND, Shacklock PS, Knight MR, Trewavas AJ (1993) Imaging calcium dynamics in living plant cells and tissues. Cell Biol Int **17**: 111-125.

Russ U, Grolig F, Wagner G (1991) Changes in cytoplasmic free Ca^{2+} in the green alga *Mougeotia scalaris* as monitored with indo-1, and their effect on the velocity of chloroplast movements. Planta **184**: 105-112.

Sheppard C (1993) Confocal microscopy - principles, practice and options. In: *Fluorescent and Luminescent Probes for Biological Activity: A Practical Guide to Technology for Quantitative Real-Time Analysis* (Mason WT, ed) Academic Press, London, pp 229-236.

Shotton DM (1989) Review: confocal scanning optical microscopy and its applications for biological specimens. J Cell Science **94**: 175-206.

Shotton DM, White NS (1989) Confocal scanning microscopy: three-dimensional biological imaging. TIBS **14**: 435-439.

Somerville CR, Somerville SC, Ogren WL (1981) Isolation of photosynthetically active protoplasts and chloroplasts from *Arabidopsis thaliana*. Plant Sci Lett **21**: 89-96.

Taylor DL, Wang Y-L (1989) Fluorescence microscopy of living cells in culture. Part B. Academic Press, San Diego, Methods Cell Biol **30**, p 503.

Thiel G, Blatt MR, Fricker MD, White IR, Millner P (1993) Modulation of K+ channels in *Vicia* stomatal guard cells by peptide homologs to the auxin-binding protein C-terminus. Proc Natl Acad Sci USA **90**: 11493-11497.

Tlalka M, Gabryš H (1993) Influence of calcium on blue-light-induced chloroplast movement in *Lemna trisulca* L. Planta **189**: 491-498.

Wang Y-L, Taylor LD (1989) Fluorescence microscopy of living cells in culture. Part A. Academic press, San Diego, Methods Cell Biol **29**, p 333.

Weyers JDB, Meidner H (1990) *Methods in Stomatal Research*. Longman, Harlow Essex, UK.

White JG, Amos WB, Fordham M (1987) An evaluation of confocal versus conventional imaging of biological structures by fluorescence light microscopy. J Cell Biol **105**: 41-48.

Williams DA (1990) Quantitative intracellular calcium imaging with laser-scanning confocal microscopy. Cell Calcium **11**: 586-597.

Williams DA, Cody SH, Gehring CA, Parish RW, Harris PJ (1990) Confocal imaging of ionised calcium in living plant cells. Cell Calcium **11**: 291-297.

Wilson T (1990) *Confocal Microscopy*. Academic Press, London.

Zhang DH, Callaham DA, Hepler PK (1990) Regulation of anaphase chromosome motion in *Tradescantia stamen* hair cells by calcium and related signalling agents. J Cell Biol **111**: 171-182.

Discussion with Reviewers

R.B. Moreton: Artifacts due to mis-registration of the two wavelength images on account of tissue movement could be further reduced if the component images are justified by reference to the bright-field image, before the ratio is constructed. All that is needed is regular recording of the bright-field image, and careful timing of the fluorescence images so that the extent of the tissue movement appropriate to each can be calculated by interpolation. It is, of course, necessary to assume the tissue moves at a uniform speed. Has this been tried ?

Authors: This approach is valid for movements relating to the whole cell or tissue using conventional wide-field imaging. It could only be applied to confocal images if the movement is restricted to the XY plane as any movement in Z would cause sampling of a different part of the specimen. It is not usually possible to detect

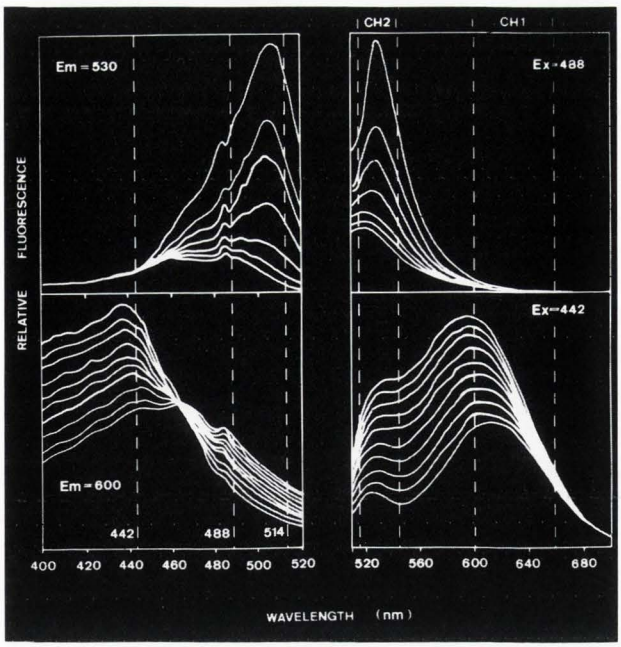

Figure 6: Excitation and emission spectra during in vitro calibration of BCECF (top panels) and Fura-Red (lower panels) using the protocols described in Materials and Methods.

movement in Z from the bright-field images as they are collected with a non-confocal transmission detector. This form of correction would also not be valid for the pollen tube example, as the movement artifact is created by the growth of the tube altering the tube morphology rather than simply a lateral displacement of the existing structure. The terminology we used to describe this particular artifact as 'mis-registration' may have been ambiguous in this context. The best means to minimise this artifact is to reduce the image collection time and the switching time between each wavelength.

C. Brownlee: How significant is the bleed-though of the Fura-Red signal into the BCECF channel, given the quantum efficiency of Fura-Red is very low ?
Authors: There is no simple answer to this problem. The spectrum of Fura-Red (Figure 6 lower right panel) has a significant shoulder that overlaps the BCECF emission (Figure 6 top right panel). The relative contribution this peak makes will depend on the concentration of the two dyes (normally 10 fold higher levels of Fura-Red are needed) and the relative pH and Ca^{2+} levels. Increasing the level of BCECF minimise the interference from Fura-Red in the 540 nm channel (CH2), but introduces problems with BCECF bleed-through into the red channel (CH1 - Figure 6).

C. Brownlee: How is intracellular dye concentration estimated ?
Authors: Dye concentrations were estimated by comparison of signals from region of cytoplasm larger that the sampling voxel volume with known dye concentrations in fluorochrome seas. For BCECF, the isosbestic wavelength provides a straightforward comparison. For the calcium dyes, the signal at the Ca^{2+}-bound wavelength after calibration was used.

N.D. Read: How common is nuclear dye compartmentation observed in the different cell types examined by the authors ?
Authors: The nucleus is characterised by a strong signal with all the dyes tested, whether loaded as AM-esters, low pH or microinjection in all of the tissues so far examined. There may be some debate as to whether this reflects compartmentation of the dye in the nucleus. The confocal sampling volume (voxel) would normally be completely contained within the nucleus whereas thin regions of cytoplasm, such as cytoplasmic strands, could be smaller than the voxel volume sampled and give proportionally lower signals. Despite this, the fluorescence signals from the nucleus are often 6-10 fold higher than the neighbouring cytoplasm, which suggests that there is active uptake of the dye, non-specific binding to nuclear components or an alteration in the fluorescence properties of the dye in the different environment within the nuclear matrix.

N.D. Read: Why was the ester-loading of *Arabidopsis* protoplasts performed on ice?
Authors: So far reduced temperatures give a more consistent cytoplasmic loading with less dye accumulation in the vacuole or loss across the plasma membrane.